Article

Synthesis and Intramolecular Energy- and Electron-Transfer of 3D-Conformeric Tris(fluorenyl-[60]fullerenylfluorene) Derivatives

He Yin [1], Min Wang [1], Loon-Seng Tan [2] and Long Y. Chiang [1,*]

[1] Department of Chemistry, University of Massachusetts Lowell, Lowell, MA 01854, USA;
He_Yin@student.uml.edu (H.Y.); wangmin81@gmail.com (M.W.)

[2] Functional Materials Division, AFRL/RXA, Air Force Research Laboratory, Wright-Patterson Air Force Base, Dayton, OH 45433, USA; loon.tan@us.af.mil

[*] Correspondence: Long_Chiang@uml.edu; Tel.: +1-978-934-3663; Fax: +1-978-934-3013

check for updates

Abstract: New 3D conformers were synthesized to show a nanomolecular configuration with geometrically branched 2-diphenylaminofluorene (DPAF-C_{2M}) chromophores using a symmetrical 1,3,5-triaminobenzene ring as the center core for the connection of three fused DPAF-C_{2M} moieties. The design led to a class of *cis-cup*-tris[(DPAF-C_{2M})-C_{60}(>DPAF-C_9)] 3D conformers with three bisadduct-analogous <C_{60}> cages per nanomolecule facing at the same side of the geometrical molecular *cis-cup*-shape structure. A sequential synthetic route was described to afford this 3D configurated conformer in a high yield with various spectroscopic characterizations. In principle, a nanostructure with a non-coplanar 3D configuration in design should minimize the direct contact or π-stacking of fluorene rings with each other during molecular packing to the formation of fullerosome array. It may also prevent the self-quenching effect of its photoexcited states in solids. Photophysical properties of this *cis-cup*-conformer were also investigated.

Keywords: Tri[60]fullerenyl stereoisomers; *cis-cup*-form of 3D-stereoisomers; tris(diphenylaminofluorene); 3D-configurated nanostructures; intramolecular energy transfer for singlet oxygen production; intramolecular electron transfer for superoxide radical production

1. Introduction

Photoinduced intramolecular energy and electron transfer phenomena in organo [60]fullerene derivatives having a covalent molecular composition of both an electron donor and a [60]fullerenyl or nanocarbon acceptor components were demonstrated over a number of years [1–3]. The energy process may involve the facile triplet state of fullerene and other chromophores [4–8]. This type of nanomolecular system was used in many technological applications [9,10], including photovoltaic devices [11,12], sensors and switches [13], and photodynamic therapy [14,15]. Fullerene-based nanostructures with multiple C_{60} cages [16] in the structure were found to be suitable for the applications of nanocars [17–19], photoswitches [20], molecular heterojunctions [21], and catalysts [22]. Unusual molecular properties of multi-cage fullerene objects were theoretically predicted [23–26]. Recently, similar photophysical chemistry was also simulated in the modulation of photoswitchable dielectric properties to observe a large amplification of dielectric constants in a material combination form of multi-layered core-shell nanoparticles (NPs) [27–29]. The latter system was based on photoinduced intramolecular electronic charge-polarization of light-harvesting chromophoric nano[60]fullerenyl conjugates, such as 9,9-di(3,5,5-trimethylhexyl)-2-diphenylaminofluorenyl-methano[60]fullerene C_{60}(>DPAF-C_9) (**1**-C_9, Figure 1). The polarization provided detectable dielectric property enhancement

in a layered [60]fullerosome membrane structure on gold-shelled nanoparticles. The phenomena were based on the high electronegativity of C_{60}> cage making it possible to rapidly shift an electron from light-harvesting DPAF (diphenylaminofluorene) donor moiety within the molecular structure to the C_{60}> moiety. This resulted in the formation of the corresponding charge-separated (CS) state $C_{60}^{-} \cdot (>DPAF-C_9)^{+}$ as the source of polarized charges. In fact, ultrafast concurrent intramolecular energy and electron transfer kinetics within **1**-C_9 were substantiated previously by femtosecond transient absorption measurements (pump-probe) [30–32]. When these negative charges were distributed, delocalized, and stabilized in the fullerosome membrane array at the shell layer on core-shell NPs, it resulted in a CS state with a lifetime prolonged enough for the detection of dielectric characteristics. The process involved interlayer photoinduced plasmonic energy transfer from the Au shell layer to the outer shell layer of $C_{60}(>DPAF-C_9)$ in addition to the fact that **1**-C_9 itself is also photoresponsive and excitable under light irradiation.

One crucial parameter to consider is the method of molecular packing within the fullerosome shell layer. In this regard, strong tendency of light-harvesting chromophores to aggregate among π-conjugated planar aromatic moieties can cause either concentration-dependent self-quenching effects of excited states or luminescence in the solid phase, including fullerosome. The π–π stacking may result in significant reduction of many photophysical properties. This type of packing aggregation can be partially minimized by the use of highly bulky and geometrically hindered π-conjugated chromophores in a structural design to restrict or distort intramolecular rotation bonding units with steric hindrance [33]. In the case of DPAF-C_9, we recently developed and synthesized highly restricted 3D conformers based on inter-connected three DPAF-C_9 chromophore units giving a structure of tris(DPAF-C_9) (**2**-C_9) [34] to prevent and minimize the tendency of planar DPAF units to undergo aromatic–aromatic stacking, overlapping, and aggregation via intermolecular hydrophobic–hydrophobic interactions in solid thin-films. This structural modification led the enhancement of photophysical properties, including the intensity of photoluminescence (PL) and electroluminescence (EL) emissions [35].
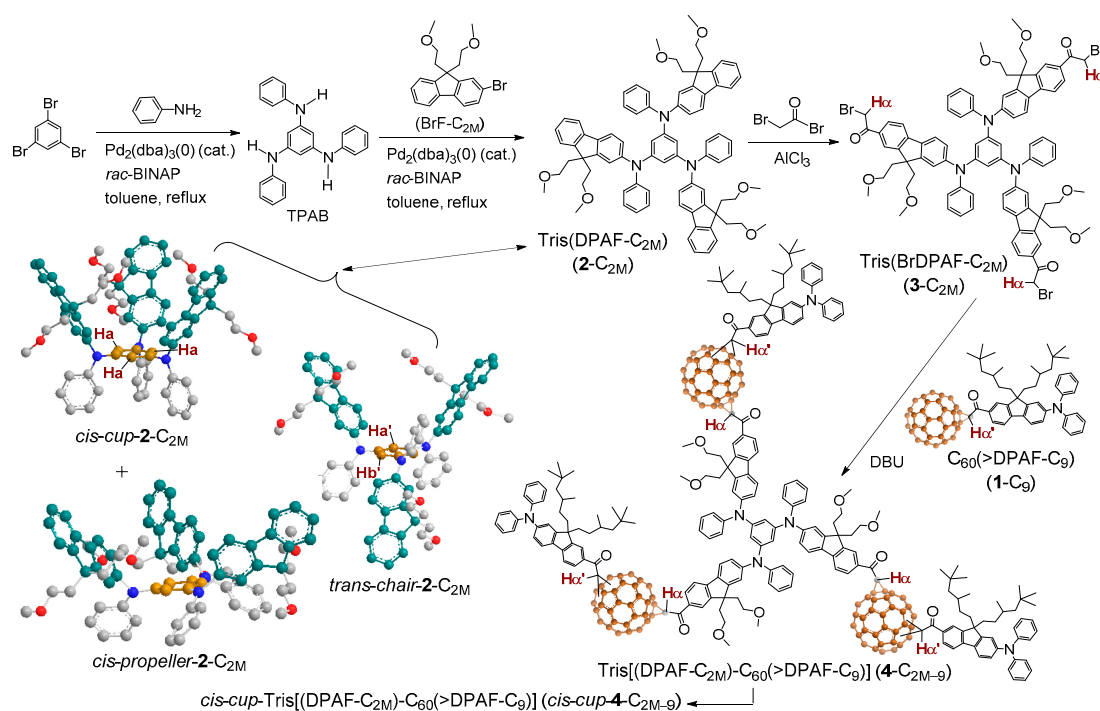
Figure 1. Synthetic methods for the preparation of 3D conformers of tris[(DPAF-C_{2M})-C_{60}(>DPAF-C_9)] (**4**-$C_{2M–9}$) with reaction reagents given and three perspective 3D-configurations of the key stereoisomeric intermediate **2**-C_{2M}.

Accordingly, we extended the similar structural strategy to design new 3D conformers tris[(DPAF-C_{2M})-C_{60}(>DPAF-C_9)] (**4**-C_{2M-9}), as shown in Figure 1, for the study. The stereochemical modification was based on the construction of 3D geometrically branched tris[(DPAF-C_{2M}) (**2**-C_{2M}) chromophore having a shared central benzene unit among three 2-diphenylaminofluorenes. Highly steric hindrance at the corresponding 1,3,5-phenylfluorenylaminobenzene moiety forced three fluorene ring moieties to twist either upward or downward away from the central benzene plane with a large torsional angle on the nitrogen atom. This resulted in the formation of three to four possible stereoisomeric configurations, such as *cis-cup*-**2**-C_{2M}, *trans-chair*-**2**-C_{2M}, and *cis/or trans-propeller*-**2**-C_{2M}, as shown in Figure 1. All of these conformer forms were proposed to be capable of fully eliminating the tendency of **4**-C_{2M-9} in inducing π–π aromatic–aromatic type stacking packing and to allow all C_{60} > cages to interact with each other via strong hydrophobic–hydrophobic interaction forces between $(C_{60}>)$–$(C_{60}>)$ fullerenyl cages, forming the nano-layer array of fullerosome membrane.

2. Results and Discussion

Rapidly responsive nanophotonic physical properties of 3D conformers tris[(DPAF-C_{2M})-C_{60}(>DPAF-C_9)] (**4**-C_{2M-9}) are achievable by specifically associating a donor–acceptor type chemical structure to a photomechanism having the ability to create a largely enhanced intramolecular energy and electron transfer efficiency. This mechanism occurs between C_{60}> acceptor and DPAF-C_{2M}/and DPAF-C_9 donor moieties bonded on fullerenes. In our functional group design of **4**-C_{2M-9}, a methanoketo bridging unit was used to trigger the keto-enol isomerization tautomerism that is capable of inducing π-periconjugation between C_{60}> and DFAP to provide a partial conjugation pathway for enhancing the π-electron mobility around the conjugated system of molecular nanostructures [36,37]. In addition, the new molecular design of stereoisomeric tris(fluorenylphenylamino)benzene [tris(DPAF-C_9)] analogous was proven to act as a fluorophore showing high intensity of photoluminescence and electroluminescence emission efficiency [34,35]. This revealed the successful utilization of stereochemistry to allow hindered and branched 3′,5′,5′-trimethylhexyl (C_9) arms to maintain the space-separation of three planar DPAF moieties intramolecularly within the nanostructure. It also behaved similarly in intermolecular packing that improved light-harvesting efficiency.

Based on the molecular formation energy based density functional theory (DFT) calculations of three plausible stereoisomers of tris(DPAF-C_9) (**2**-C_9) via B3LYP/6-31G* level of theory using SPARTAN08 [34,35], the results revealed high stability of the *cis-cup*-form with other forms in stability order of *cup* > *chair* > *propeller*, as shown in Figure 1. This agreed well for the alkyl n-C_6, n-C_7, and n-C_8 substituents owing to the influence by strong dispersion interactions within the alkyl chains. In the case of the methyl and the ethyl substituents, *trans-chair*-form may have been more stable than *cis-cup*-form. Accordingly, three C_4-analogous substituents of tris(DPAF-C_{2M}) (**2**-C_{2M}) facing toward each other in the 3D molecular space above the central benzene ring should have brought in the minimum alkyl–alkyl interaction forces required to keep a slight favor of the *cis-cup*-form over either *trans-chair*- or *cis/trans-propeller* form.

Synthetically, the precursor molecule 2-bromo-9,9-bis(methoxyethyl)fluorene (BrF-C_{2M}) was prepared by alkylation of 2-bromofluorene with mesylated methoxyethanol reagent using potassium *t*-butoxide as a base in a high yield of 90% (Figure 1). The key 3D-conformeric intermediate **2**-C_{2M} was synthesized by the reaction of BrF-C_{2M} with 1,3,5-tris(phenylamino)benzene (TPAB) in the presence of sodium *t*-butoxide, a catalytic amount of tris(dibenzylideneacetone)dipalladium(0) [$Pd_2(dba)_3(0)$], and *rac*-2,2′-bis(diphenylphosphino)- 1,1′-binaphthyl (*rac*-BINAP, 0.75 mol%) in anhydrous toluene at reflexing temperature for a period of 72 h to yield 82% of the product as a light yellow solid after chromatographic purification [SiO_2, hexane–ethylacetate (1:1, *v/v*) as the eluent]. Subsequent attachment of three C_{60}(>DPAF-C_9) (**1**-C_9) on **2**-C_{2M} should have led to the nanostructure of tris[(DPAF-C_{2M})-C_{60}(>DPAF-C_9)] (**4**-C_{2M-9}) having all **1**-C_9 moieties extended outward from the central 1,3,5-triaminobenzene core. Prior to the attachment of three **1**-C_9 on **2**-C_{2M}, it was functionalized by the Friedel–Crafts acylation at C7 position of 2-diphenylaminofluorene moiety [36]

with excessive α-bromoacetyl bromide (11.4 equiv.) in the presence of aluminum chloride (17 equiv.) in 1,2-dichloroethane at 0–10 °C to ambient temperature overnight to afford the corresponding α-bromoacetylfluorene derivative in this intermediate step of reactions. It resulted in viscous yellow semi-solids in 48% yield of tris(BrDPAF-C_{2M}) (**3**-C_{2M}). It was purified by either column or thin-layer chromatography (TLC) [silica gel, hexane–EtOAc (1:1, *v/v*) as eluent, R_f = 0.5 on TLC]. The final step of synthesis for the preparation of 3D-conformers **4**-C_{2M-9} was performed by the reaction of **3**-C_{2M} with **1**-C_9 (5.0 equiv.) in the presence of 1,8-diazabicyclo[5.4.0]undec-7-ene (DBU) in toluene at room temperature for 8.0 h. During the first Bingel reaction period of 2.0 h, mono- and bis-adducts could be observed and detected by the TLC technique, showing two brown fraction bands (R_f = 0.2 and 0.3 on TLC plate, corresponding to mono- and bis-adducts, respectively). Subsequently, three brown fraction bands (R_f = 0.2, 0.3, and 0.4) appeared after 4 h of reaction, indicating sequential additions of C_{60}(>DPAF-C_9) on the starting substrate tris(BrDPAF-C_{2M}) (**3**-C_{2M}) with the R_f band at 0.2 gradually disappeared. At the end of the reaction, only two bands (R_f = 0.3 and 0.4) remained, with the latter being identified as a major product band of **4**-C_{2M-9}. After purification of this fraction by column chromatography (silica gel) using toluene–ethyl acetate (7:3) as the eluent, the brown solids of tris[(DPAF-C_{2M})-C_{60}(>DPAF-C_9)] were obtained in 79% yield.

The compound **4**-C_{2M-9} exhibited good solubility in common organic solvents owing to its possession of three DPAF-C_9 (with a total of six branched C_9-alkyl groups) and three DPAF-C_{2M} (with a total of six methoxyethyl groups) moieties (Figure 1), making three C_{60}> cages become encapsulated in the center of the 3D molecular configuration. The 3D configuration of *cis-cup* form resulted in these alkyl groups being the main structural moieties interacting with the solvent. Accordingly, the compound had solubility (20 mg/mL in $CHCl_3$ or CH_2Cl_2) over 10 times higher than that of C_{60} itself in toluene (1.4 mg/mL).

2.1. Spectroscopic Characterization of Synthetic 3D Configured Fullerenyl Nanomaterials

All chemical conversions of intermediate chemicals to the corresponding products at each step of the reactions were characterized by various spectroscopic techniques. The functional attachment of three α-bromoaceto groups (3.0 equiv.) to tris(DPAF-C_{2M}) given the product of tris(BrDPAF-C_{2M}) was verified by both infrared (FT-IR) and ^{1}H-NMR spectra. The former showed a new strong carbonyl (–C=O) stretching absorption band centered at 1673 cm^{-1}, indicating each of the three carbonyl groups being bonded on a phenyl moiety, such as that of **2**-C_{2M}. This absorption wavelength was in clear contrast to the strong band absorption at 1725 cm^{-1} normally detectable for an alkyl carbonyl group. In the case of ^{1}H-NMR spectrum, tris(BrDPAF-C_{2M}) displayed characteristic new peak signals of three methylene protons (H_α) next to the carbonyl group of the α-bromoaceto moiety at δ 4.49 (Figure 2Ab) as compared with that of **2**-C_{2M} (Figure 2Aa). Subsequent attachment of three C_{60}(>DPAF-C_9) moieties to each of the three DPAF moieties of **3**-C_{2M} with a cylopropylaceto bridging unit on each C_{60}> cage of three **1**-C_9 (applied as a reagent) showed evidence of changing solubility characteristics of the product **4**-C_{2M-9} matching with those of **1**-C_9. Its FTIR spectrum displayed a slight shift of cyclopropyl keto group absorption band to ν_{max} 1679 cm^{-1} (Figure 3d), which was assigned to the carbonyl (C=O) stretching band. It was also accompanied by an olefinic (C=C) absorption band centered at ν_{max} 1591 cm^{-1}. Both C=O and C=C bands were correlated to those of C_{60}(>DPAF-C_9) (Figure 3b) and tris[C_{60}(>DPAF-C_9)] (Figure 3c), showing a nearly identical absorption wavenumber. Most importantly, we were able to detect two typical fullerenyl cage bands at ν_{max} 574 (w) and 524 (s) cm^{-1} (Figure 3d). These two bands were corresponding characteristic absorptions used to provide evidence of (C_{60}>)-related monoadducts and bisadducts with absorption wavenumbers and relative intensity ratios differentiable from those of C_{60} (Figure 3a) and **1**-C_9 substituents (Figure 3b). Accordingly, we applied this IR technique for the product structure verification during the chemical conversion from **3**-C_{2M} to **4**-C_{2M-9}. Upon conversion of C_{60} to its monoadducts, such as those of Figure 3b,c, the remaining cage structure of C_{60}> exhibited the same two bands with a reduced peak intensity for the 574 cm^{-1} band. The intensity of this band was further reduced in the structure of

<C$_{60}$>-like bisadduct, such as **4**-C$_{2M-9}$ (Figure 3d). Furthermore, the latter band at 524 cm^{-1} still remaining strong was indicative of successful attachment of C$_{60}$(>DPAF-C$_9$) moieties on **3**-C$_{2M}$ due to the possibility of having the second malonate bridging unit being attached at or near the equator region of the C$_{60}$> cage. This would have led to the retention of a C$_{60}$ half-cage that enabled absorption at 524 cm^{-1}.
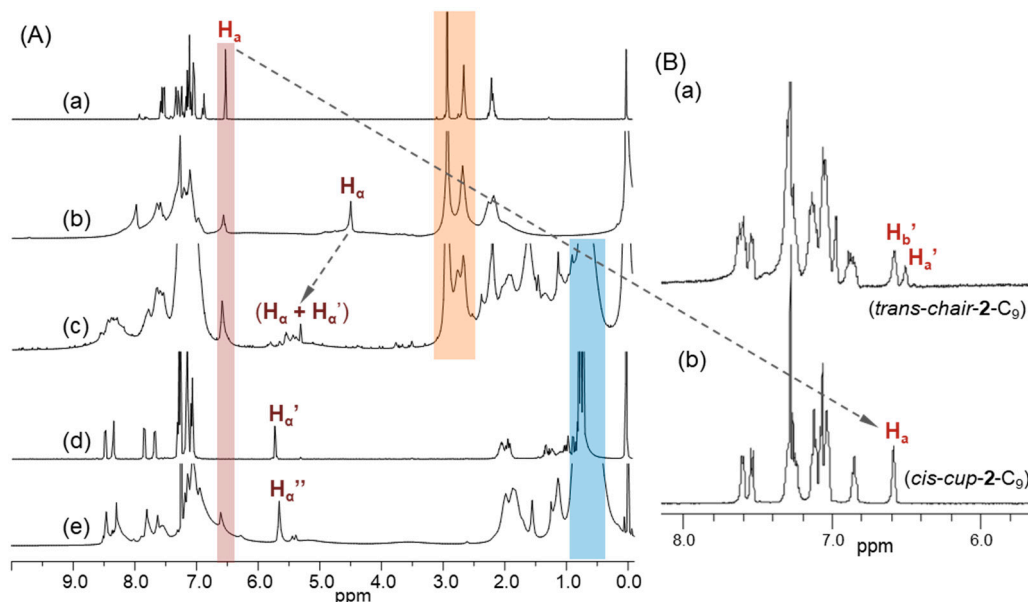
Figure 2. ^{1}H-NMR spectra (CDCl$_3$) of (**A**) (a) tris(DPAF-C$_{2M}$) (**2**-C$_{2M}$), (b) tris(BrDPAF-C$_{2M}$) (**3**-C$_{2M}$), (c) tris[(DPAF-C$_{2M}$)-C$_{60}$(>DPAF-C$_9$)] (**4**-C$_{2M-9}$), (d) C$_{60}$(>DPAF-C$_9$) (**1**-C$_9$), and (e) tris[C$_{60}$(>DPAF-C$_9$)]. (**B**) ^{1}H-NMR spectra (CDCl$_3$) of (a) *trans-chair*-tris(DPAF-C$_9$) (*trans-chair*-**2**-C$_9$) and (b) *cis-cup*-tris(DPAF-C$_9$) (*cis-cup*-**2**-C$_9$) for comparison.
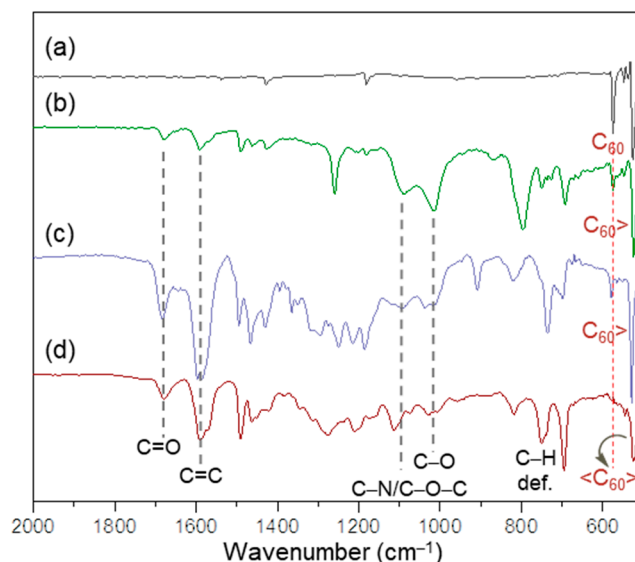
Figure 3. Infrared spectra (KBr) of (a) C$_{60}$, (b) C$_{60}$(>DPAF-C$_9$) (**1**-C$_9$), (c) tris[C$_{60}$(>DPAF-C$_9$)]. and (d) tris[(DPAF-C$_{2M}$)-C$_{60}$(>DPAF-C$_9$)] (**4**-C$_{2M-9}$).

By the analysis of ^{1}H-NMR spectrum, disappearance of peaks corresponding to the chemical shift of α-proton (H$_\alpha$) on the α-bromoaceto group of **3**-C$_{2M}$ at δ 4.49 (Figure 2Ab) along with the appearance of new peaks over δ 5.25–5.78 (Figure 2Ac) provided evidence of successful formation of a cyclopropanyl keto-bridging unit between a C$_{60}$> cage and the fluorene moiety. By using the previously

reported chemical shift values of the α-proton (H$_\alpha$') in C$_{60}$(>DPAF-C$_9$) (Figure 2Ad) [20] and the related α-proton (H$_\alpha$'') in tris(DPAF-C$_9$) (**2**-C$_9$, Figure 2Ae) [23] as the reference, we assigned these proton peaks to a combination of H$_\alpha$ and H$_\alpha$'. A large downfield shift of the H$_\alpha$ chemical shift from those of **3**-C$_{2M}$ at δ 4.49 to δ 5.25–5.78 for **4**-C$_{2M-9}$ provided clear evidence of three C$_{60}$(>DPAF-C$_9$) moieties being attached on the corresponding α-bromoaceto bridging units of **3**-C$_{2M}$. The characteristics of the multipeaks for H$_\alpha$ and H$_\alpha$' revealed a less symmetrical environment among these six protons of **4**-C$_{2M-9}$ as the geometric shape of the nanostructure extended to a 3D configuration. It is worthwhile to mention that a large down-fielded chemical shift value of either H$_\alpha$' or H$_\alpha$'' away from the normal value of δ 2.1–2.5 for an alkyl aceto-α-proton was caused by the influence of strong [60]fullerenyl ring current in close vicinity. In addition, the alkyl proton regions over δ 2.93 (methoxy proton, 18H) and δ 2.75–2.64 (ethylenoxy proton, 12H) of Figure 2Ac (marked by beige) were correlated well to those of **2**-C$_{2M}$ at δ 2.91 (18H) and δ 2.64 (12H) (Figure 2Aa), respectively, indicating good retention of central tris(DPAF-C$_{2M}$) core region without any structural change of methoxy groups during the Friedel–Crafts acylation reaction. It also showed a new group of methyl proton peaks at δ 0.30–2.07 having an integration ratio value of 113.28, which represented 114 fluorenyl protons of C$_9$-alkyl proton (19Hs for each of the two C$_9$-alkyls of DPAF-C$_9$) and was indicative of six C$_9$-alkyl groups in the structure, consistent with the product structure. Additional ^{1}H-NMR spectroscopic data analyses on proton integrations of all proton peaks to substantiate and count for the molar quantity ratio among fluorene, methoxyethyl, and C$_9$ alkyl moieties to prove the molecular formulation of **4**-C$_{2M-9}$ are provided in supporting information.

Most importantly, characteristics of central benzene protons at the core region could be used for the analysis of the relatively geometric configuration of three fluorenyl rings with respect to each other. With a symmetrical structure of TPAB, three benzene protons should have displayed a singlet peak in its ^{1}H-NMR spectrum. Upon attachment of a bulky fluorenyl moiety at each diphenylamino group, it induced high torsional stress and steric hindrance at the nitrogen atom that forced each 9,9'-di(methoxyethyl)fluorene moiety to twist or rotate either upward or downward from the central benzene plane. The action resulted in two main 3D conformers: *cis-cup*-**2**-C$_{2M}$ and *trans-chair*-**2**-C$_{2M}$. The former with three C$_{60}$(>DPAF-C$_9$) moieties facing upward on the same side in the structure gave a singlet H$_a$ peak (Figure 1). The latter with one facing downward and two C$_{60}$(>DPAF-C$_9$) moieties facing upward in the structure resulted in two proton peaks for *trans*-H$_a$' (1H) and *trans*-H$_b$' (2H) (Figure 2Ba). By analyzing Figure 2Aa of tris(DPAF-C$_{2M}$), a sharp singlet proton peak at δ 6.53 was assigned to the chemical shift of central benzene proton *cis*-H$_a$. This peak was compared with that of the H$_a$ proton peak of *cis-cup*-tris(DPAF-C$_9$) (*cis-cup*-**2**-C$_9$, Figure 2Bb) showing even better resolution of the peak profile, indicating a high purity of one 3D conformer fraction in a *cis-cup*-**2**-C$_{2M}$ form. Surprisingly, this conformer fraction was, in fact, the major product. Apparently, the hydrophobic–hydrophobic dispersion interaction forces derived from three methoxyethyl chains and heteroatoms were stronger than those among all C$_4$-alkyl groups, which led to higher tendency in formation of the *cis-cup*-form. Accordingly, subsequent attachment of three C$_{60}$(>DPAF-C$_9$) moieties on *cis-cup*-**2**-C$_{2M}$ led to a similar formation of corresponding *cis-cup*-tris[(DPAF-C$_{2M}$)-C$_{60}$(>DPAF-C$_9$)] (*cis-cup*-**4**-C$_{2M-9}$), all having **1**-C$_9$ moieties facing upward from the central benzene core at the same side with respect to each other. Additional structural analyses and discussions are provided in supporting information.

In the case of the potential formation of regio-isomers of **4**-C$_{2M-9}$ at the <C$_{60}$> moiety, since the monoadduct structure of C$_{60}$(>DPAF-C$_9$) was well-defined, with the assistance of X-ray single crystal structural analysis of C$_{60}$(>DPAF-C$_2$) [31,36], its attachment on tris(BrDPAF-C$_{2M}$) (**3**-C$_{2M}$) was believed to be governed by the bulkiness and the steric hindrance of both relatively large entities to result in only a limited number of region isomers on the C$_{60}$ cage. This was proven by the ^{1}H-NMR spectrum of **4**-C$_{2M-9}$ showing only several H$_\alpha$ and H$_\alpha$' proton peaks at roughly δ 5.2–5.8 (Figure 2Ac) instead of the broad band normally seen for the existence of a large number of region isomers. To our surprise, a peak at 524 cm^{-1} assigned the characteristic infrared absorption band of a half-C$_{60}$ cage (as stated above) showed close resemblance to those of the monoadduct C$_{60}$(>DPAF-C$_9$) (Figure 3b) and

tris[C_{60}(>DPAF-C_9)] (Figure 3c) at an identical wavenumber. This implied the structure of the major regio-isomeric products had both addend moieties located at the same half-sphere of a C_{60} cage that left the other half-sphere of C_{60} untouched.

2.2. Photophysical and Physical Properties of 3D Conformeric Fullerenyl Nanomaterials

Photophysical properties of the 3D conformer *cis-cup*-**4**-C_{2M-9} were compared with those of precursor intermediates using the UV-vis spectroscopic technique. They were governed by two photoresponsive moieties, including three electron (e^-)-accepting fullerene cages and six light-harvesting DPAF antenna units as electron (e^-)-donors. The use of the latter was to enhance the optical absorption capability at longer visible wavelengths. The absorption wavelength could be varied and modulated by the appropriate chemical modification of functional substituents on fluorenyl moiety to affect electron-pushing (donating) and pulling (accepting toward the molecular edge of C_{60}> cage moiety) mobility across the molecular π-conjugation system. As shown in Figure 4Ae of *cis-cup*-**4**-C_{2M-9}, optical absorption of C_{60}> cage moieties appeared mainly at the broad band centered at 296 nm (1.82×10^5 L mol^{-1} cm^{-1}), whereas the band centered at 411 nm (1.11×10^5 L mol^{-1} cm^{-1}) was attributed to the absorption of DPAF moieties. Characteristics of the latter band were compared with those of tris(DPAF-C_{2M}) (Figure 4Aa), tris(BrDPAF-C_{2M}) (Figure 4Ab), *cis-cup*-tris[C_{60}(>DPAF-C_9)] (Figure 4Ac), and C_{60}(>DPAF-C_9) (**1**-C_9, Figure 4Ad), showing a clear bathochromic shift of the 351 nm band of **2**-C_{2M} to 406 nm (7.91×10^4 L mol^{-1} cm^{-1}) of **3**-C_{2M}, which matched roughly with the 404 nm band of **1**-C_9 and the 402 nm band *cis-cup*-tris[C_{60}(>DPAF-C_9)] for the peak assignment. This assignment was also consistent with the observation of roughly equal absorption extinction coefficient (ε) values for **2**-C_{2M}, **3**-C_{2M}, and tris[C_{60}(>DPAF-C_9)] with the same three DPAF moieties per molecule. Upon the attachment of three C_{60}(>DPAF-C_9) moieties, optical absorptions of [60]fullerene moieties of *cis-cup*-**4**-C_{2M-9} (Figure 4Ae) at 296 nm became dominant in the spectrum with a higher ε value. It was accompanied by a weak characteristic (forbidden) steady state absorption band of the C_{60}> moiety appearing at 692 nm (the insert of Figure 4A) with a slightly higher extinction coefficient for the monoadduct **1**-C_9 than the bisadduct *cis-cup*-**4**-C_{2M-9}, which was also consistent with the photophysical property discussion above and provided further confirmation of a conjugated fullerenyl nanostructure.
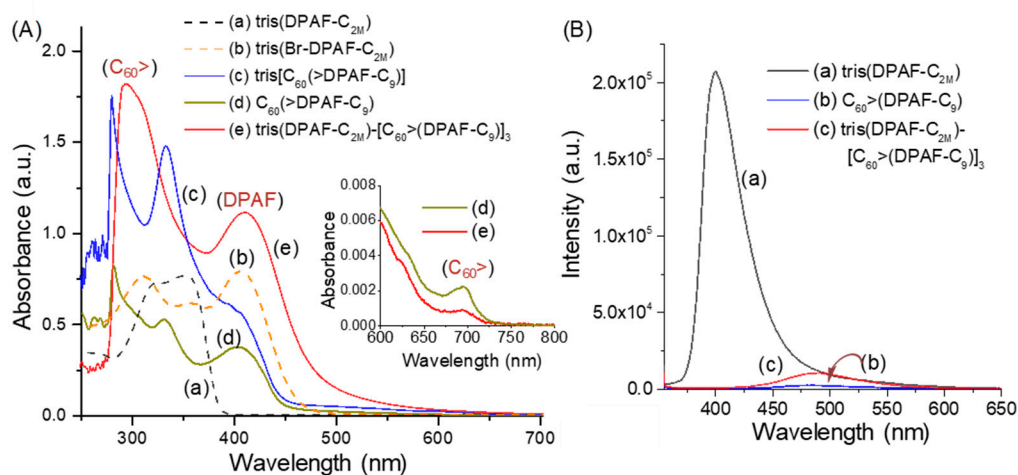
Figure 4. UV-vis spectra of (**A**) (a) tris(DPAF-C_{2M}) (**2**-C_{2M}), (b) tris(BrDPAF-C_{2M}) (**3**-C_{2M}), (c) *cis-cup*-tris[C_{60}(>DPAF-C_9)], (d) C_{60}(>DPAF-C_9) (**1**-C_9), and (e) *cis-cup*-**4**-C_{2M-9}, where (a), (b), and (e) were taken in CDCl$_3$ and (c) and (d) were taken in toluene. (**B**) Fluorescence spectra of (a) tris(DPAF-C_{2M}) (λ_{ex}: 352 nm), (b) C_{60}(>DPAF-C_9) (λ_{ex}: 406 nm), and (c) *cis-cup*-**4**-C_{2M-9} (λ_{ex}: 410 nm). The concentration of all samples is 1.0×10^{-5} M.

In addition, a roughly 2.1-fold higher ε value (1.11×10^5 L mol^{-1} cm^{-1}) of the 411 nm peak in Figure 4Ae compared to that of 404 nm band of *cis-cup*-tris[C_{60}(>DPAF-C_9)] was consistent with a

double number of DPAF arms per molecule for the former. Furthermore, very efficient intramolecular energy transfer from the excited singlet state of DPAF-C_9 antenna to $C_{60}>$ was detected, which nearly eliminated the fluorescence of $C_{60}(>$DPAF-$C_9)$ (λ_{ex}: 406 nm, Figure 4Bb). In high contrast, without any $C_{60}>$ cage in the structure, the compound of tris(DPAF-C_{2M}) showed a strong intensity of fluorescence emission (λ_{ex}: 352 nm, Figure 4Ba) that clearly indicated the loss of photoexcited energy being associated with the influence of [60]fullerene. With an additional DPAF-C_9 antenna in the structure of **4**-C_{2M-9}, it began to experience a slightly excessive fluorescence emission (λ_{ex}: 410 nm, Figure 4Bc) after the majority of photoexcited DPAF-C_{2M} energy underwent direct intramolecular energy transfer to the closely bonded [60]fullerene cage.

In investigating the plausibility of photoinduced intramolecular electron (e^-)-transfer capability within the nanostructure of the 3D conformer *cis-cup*-tris[(DPAF-C_{2M})-$C_{60}(>$DPAF-$C_9)$] (*cis-cup*-**4**-C_{2M-9}), we first investigated the unit character of redox potentials among all structural components, including the bisadduct-based $<C_{60}>$ cage and the DPAF-C_9 moieties for comparison using the cyclic voltammetric (CV) technique. Several CV measurements were performed on the sample of *cis-cup*-**4**-C_{2M-9} in a solution of CH_2Cl_2 containing $(n\text{-butyl})_4N^+\text{-}PF_6^-$ as the electrolyte and Pt as both the working and the counter electrodes and with Ag/AgCl as the reference electrode.

To deliver appropriate redox potential analyses and data interpretation, related CV characteristics of a C_{60}-bisadduct of $C_{60}(>t\text{-Bu-malonate})_2$ with a $<C_{60}>$ cage attached by two *t*-butylmalonate groups and the precursor compound $C_{60}(>$DPAF-$C_9)$ were collected. They were performed under the same CV condition over cyclic oxidation and reduction voltages versus Ag/Ag^+ from -2.0 to 2.0 V as those for *cis-cup*-**4**-C_{2M-9}, as shown in Figure 5. As a result, it displayed one reversible oxidation ($^1E_{ox}$ of 1.51 V) reduction ($^1E_{red}$ of 1.32 V) cyclic wave with the first half wave oxidation potential ($^1E_{1/2,ox}$) of 1.42 V for the DPAF moieties of *cis-cup*-**4**-C_{2M-9} at positive voltages (Figure 5Ab,Bb). In the negative voltage region, its CV diagram displayed three reversible reductions at -0.34 ($^1E_{red}$), -0.82 ($^2E_{red}$), and -1.29 V ($^3E_{red}$) with the corresponding cyclic oxidation waves at -0.15 ($^1E_{ox}$), -0.44 ($^2E_{ox}$), and -0.96 ($^3E_{ox}$), respectively. These data corresponded to the first to the third half wave reduction potentials of -0.25 ($^1E_{1/2,red}$), -0.63 ($^2E_{1/2,red}$), and -1.12 V ($^3E_{1/2,red}$), respectively. By comparison of these values to those of $C_{60}(>t\text{-Bu-malonate})_2$ (Figure 5Aa,Ba) for the fullerene cage moiety and those of $C_{60}(>$DPAF-$C_9)$ (Figure 5Ac,Bc) for both DPAF and fullerene cage moieties, highly consistent and reproducible redox potential characteristics among structural components were found that also substantiated the structural derivatization of tris[(BrDPAF-C_{2M}) (**3**-C_{2M}) with triple $C_{60}(>$DPAF-$C_9)$ to form *cis-cup*-**4**-C_{2M-9}. Accordingly, the latter exhibited combined CV characteristics of $<C_{60}>$ and DPAF-C_9. These CV characteristics were reproducible for four repeated redox cycles with the reductive $C_{60}>$ and the oxidative DPAF potential profiles showing only slight changes at the potential range of -2.0 to 2.0 V. This implied good stability of the material under CV conditions that led to possible reuse of **4**-C_{2M-9}.
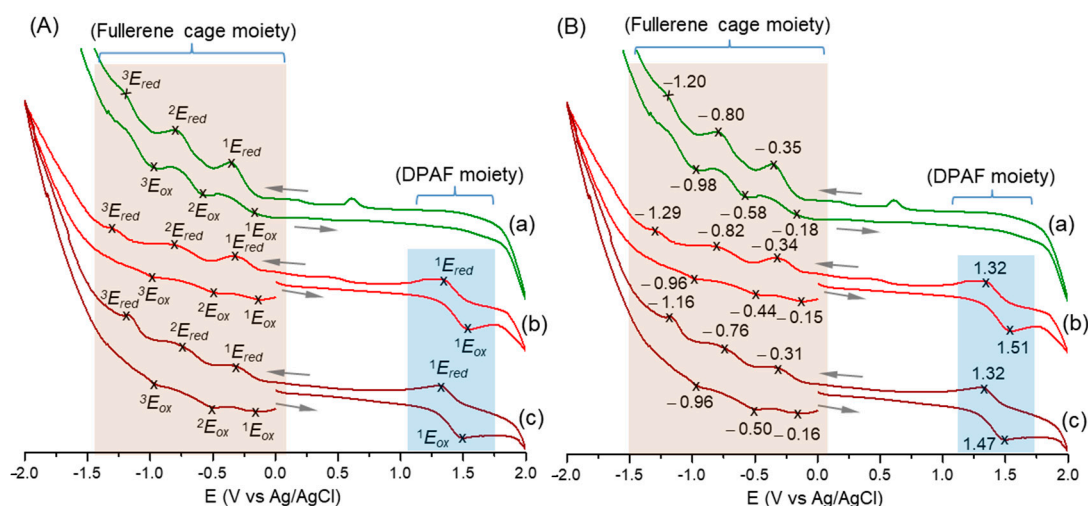
Figure 5. Cyclic voltammograms (CV) of (a) $C_{60}(>t\text{-Bu-malonate})_2$, (b) *cis-cup*-tris[(DPAF-C_{2M})-$C_{60}(>\text{DPAF-C}_9)$], and (c) $C_{60}(>\text{DPAF-C}_9)$, where (**A**) displays the sequential redox cycles of each compound with the assignments and (**B**) shows the corresponding potential voltage values at either the peak maximum or minimum of each redox cycle. All solutions were in a concentration of 5.0×10^{-3} M in CH_2Cl_2 using $(n\text{-butyl})_4N^+\text{-PF}_6^-$ as the electrolyte (0.1 M), Pt as working and counter electrodes, and Ag/AgCl as the reference electrode at a scan rate of 10 mV/s.

2.3. Evidence of Intramolecular Energy- and Electron-Transfer Events within cis-cup-4-C_{2M-9} by Detection of Corresponding Reactive Oxygen Species (ROS)

There is an appropriate approach to substantiate intramolecular energy and electron transfer events within the nanomolecular structure of *cis-cup*-**4**-C_{2M-9} by directly detecting the photoinduced production of reactive oxygen species (ROS). In general, the most common ROS includes singlet oxygen ($^1O_2$) produced by the Type-II photomechanism via the intermolecular transfer of triplet energy to molecular oxygen (O_2) and superoxide radical ($O_2^-\cdot$) generated by the intermolecular transfer of electron (e^-) to O_2. For the former case, upon photoexcitation at the $C_{60}>$ cage moiety of *cis-cup*-**4**-C_{2M-9}, the singlet excited state of bis-methanofullerenyl $^1(<C_{60}>)^*$ may undergo facile intersystem crossing in a nearly quantitative efficiency to its triplet excited state $^3(<C_{60}>)^*$ that can be accounted for by the efficient production of $^1O_2$ via Type-II triplet energy transfer processes. Alternatively, if the photoexcitation process is aimed at either the DPAF-C_{2M} or the DPAF-C_9 moiety of *cis-cup*-**4**-C_{2M-9}, the resulting corresponding singlet excited states of either $^1(\text{DPAF-C}_{2M})^*$ or $^1(\text{DPAF-C}_9)^*$ may undergo both pathways of (1) intramolecular energy transfer from either $^1(\text{DPAF-C}_{2M})^*$ or $^1(\text{DPAF-C}_9)^*$ to the $<C_{60}>$ moiety to produce neutral DPAF-C_{2M} or DPAF-C_9 and $^1(<C_{60}>)^*$, respectively; (2) intramolecular electron (e^-)-transfer from either $^1(\text{DPAF-C}_{2M})^*$ or $^1(\text{DPAF-C}_9)^*$ to the $<C_{60}>$ moiety to produce cationic $(\text{DPAF-C}_{2M})^+\cdot$ or $(\text{DPAF-C}_9)^+\cdot$ and $(<C_{60}>)^-\cdot$, respectively. Both events of (1) and (2) can occur concurrently. Subsequent intermolecular e^--transfer from $(<C_{60}>)^-$ to O_2 produces the corresponding neutral $<C_{60}>$ and O_2^- following the Type-I photomechanism.

Accordingly, by the direct detection of ROS on either $^1O_2$ and/or $O_2^-\cdot$ upon irradiation on *cis-cup*-**4**-C_{2M-9} at either $<C_{60}>$ or DPAF-C_{2M}/DPAF-C_9 moiety, we were able to provide the evidence of intramolecular energy and electron transfer processes happening within this 3D-conformer. We selected two reliable fluorescent (FL) probes for the detection of either $^1O_2$ or $O_2^-\cdot$ separately in the solution of *cis-cup*-**4**-C_{2M-9} with high selectivity and specificity as a crucial measure. To detect the former ROS $^1O_2$, a synthetic highly fluorescent compound α,α'-(anthracene-9,10-diyl)-bis(methylmalonic acid) (ABMA) was used as the probe in the experiment. Its UV-vis absorption and fluorescence emission spectra are given in Figure 6a,b, respectively. In the probe reaction, chemical trapping of $^1O_2$ by highly fluorescent ABMA resulted in the formation of non-fluorescent 9,10-endoperoxide product ABMA-O_2 (Figure 7A). This chemical conversion allowed us to follow the intensity loss of fluoresce

emission upon photoexcitation. The loss could be associated with the proportional quantity of $^1O_2$ produced. The correlation was valid owing to a higher reaction kinetic rate of the trapping process in solution than the internal decay of $^1O_2$ in the same solvent system of a DMF–CHCl$_3$ (1:9, *v/v*) mixture. Experimentally, the quantity of $^1O_2$ generated was monitored and counted by the relative intensity decrease of fluorescence emission (λ_{em}) of ABMA at 428 nm under excitation wavelength (λ_{ex}) of 380 nm. At this excitation wavelength, it matched partially with the optical absorption band of DPAF moieties of *cis-cup*-**4**-C$_{2M-9}$ that led to a slight fluorescence emission (Figure 6c) after the intramolecular energy and the e$^-$-transfer processes. It gave a slightly higher count in the overall FL intensity during the experiment (Figure 6d). In a typical probe reaction, a master solution of ABMA in DMF was diluted by CHCl$_3$ prior to the addition of *cis-cup*-**4**-C$_{2M-9}$. It was followed by periodical illumination using a light emitting diode (LED) lamp of white light (a power output of >2.0 W) operated at two major emission peak maxima (λ_{max}) centered at 451 and 530 nm. The former light emission spectrum exhibited a sufficient bandwidth covering the 410–470-nm region for photoexcitation of DPAF moieties with optical absorption bands covering 380–500-nm (Figure 4Ae). As a result, we were able to detect rapid production of $^1O_2$ by *cis-cup*-**4**-C$_{2M-9}$ upon irradiation in a decreasing curve profile over a period of more than 120 min (Figure 7Ab).
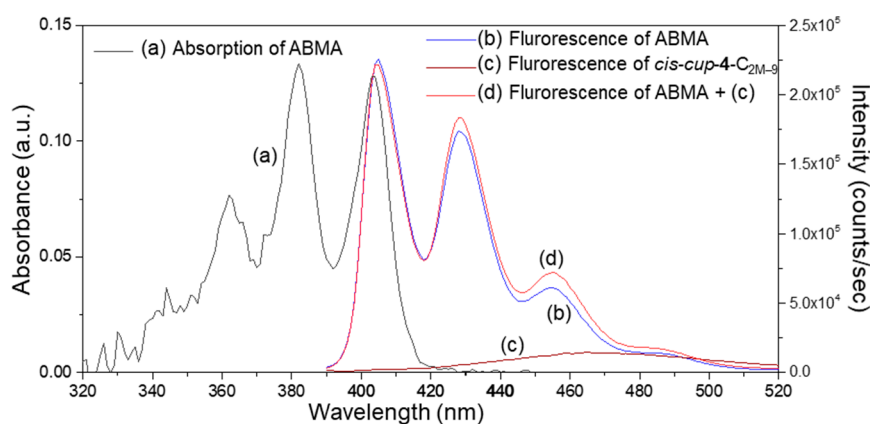
Figure 6. (a) UV-vis spectra of *α,α'*-(anthracene-9,10-diyl)bis(methylmalonic acid) (ABMA) and fluorescence (FL) emission spectrum of (b) ABMA, (c) *cis-cup*-tris[(DPAF-C$_{2M}$)-C$_{60}$(>DPAF-C$_9$)] (*cis-cup*-**4**-C$_{2M-9}$), and (c) a combination of ABMA and *cis-cup*-**4**-C$_{2M-9}$ in a solvent mixture of DMF–CHCl$_3$ (1:9, *v/v*) in a concentration of 10^{-6} M.

The FL probe experiments were calibrated by a blank control run using the same probe concentration of ABMA alone and an illumination time scale in the absence of *cis-cup*-**4**-C$_{2M-9}$ (Figure 7Aa). Apparently, we observed slight photodegradation of ABMA itself. This may have implied the existence of a photoinduced triplet state of ABMA in a low quantity due to exposure to short wavelength regions of the light emission bandwidth covering over ~380 nm of ABMA absorption bands.
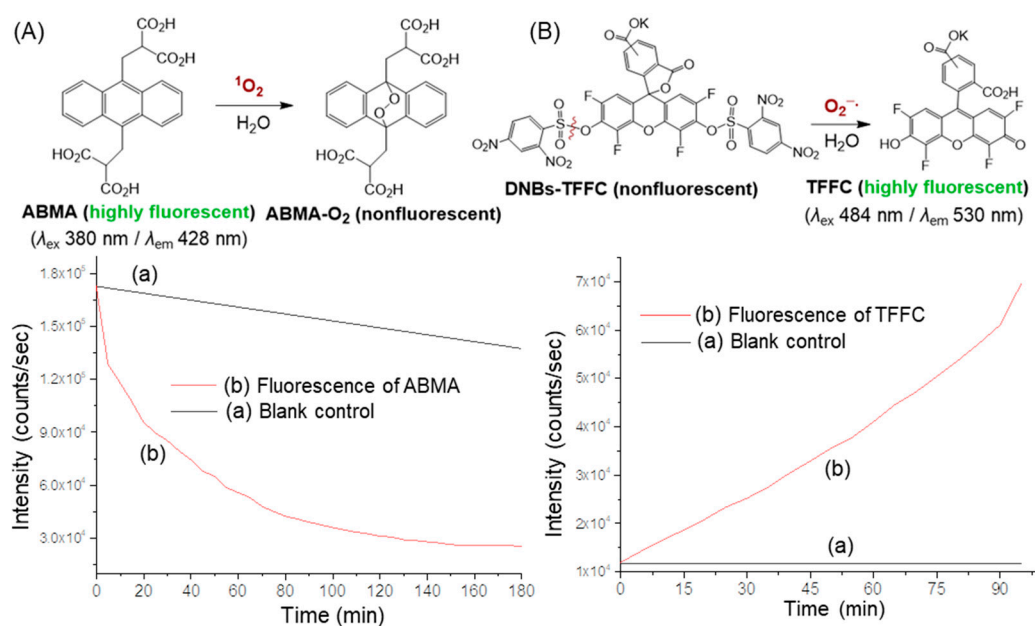
Figure 7. Fluorescence (FL) emission spectra of (**A**) ABMA and (**B**) tetrafluorofluorescein-10′ (or 11′)-carboxylate (TFFC) to correlate directly the singlet oxygen ($^1O_2$) and superoxide radical (O_2^-·) production efficiency, respectively, with (a) blank control and (b) a mixture of corresponding probe and *cis-cup*-**4**-C$_{2M-9}$ samples in DMF–CHCl$_3$ (1:9, *v/v*) at a concentration of 1.0×10^{-5} M using ABMA as the $^1O_2$ trapping agent at λ_{ex} 350 nm and λ_{em} 428 nm and DNBs-TFFC as the O_2^-·-acceptor agent at λ_{ex} 484 nm and λ_{em} 530 nm for detection with the irradiation of white light emitting diode (LED) light.

In the case of detecting superoxide radical as the second ROS, a synthetic O_2^-·-reactive fluorescent probe precursor molecule, non-fluorescent potassium bis(2,4-dinitrobenzenesulfonyl)-2′,4′,5′,7′-tetrafluorofluorescein-10′ (or 11′)-carboxylate (DNBs-TFFC), was applied for the experiment. Its molecular structure was synthetically modified from that reported previously [38], showing good reaction selectivity with a high O_2^-·/$^1O_2$ sensitivity ratio. Since DNBs-TFFC itself is photodegradable, a dialysis film with the molecular weight cut-off (MWCO) of 100–500 Daltons was applied to hold the solution of *cis-cup*-**4**-C$_{2M-9}$ in toluene–DMSO (9:1, *v/v*). The sack bag was separated from the solution of the probe DNBs-TFFC. The latter was kept in a cuvette with stirring during the fluorescence emission measurement. Only the solution of *cis-cup*-**4**-C$_{2M-9}$ in the dialysis membrane sack was subjected to the white LED light exposure. Any superoxide radical produced was allowed to rapidly diffuse into the probe solution through the dialysis membrane and initiate the desulfonylation of DNBs-TFFC. The O_2^-·-trapping reaction led to the elimination of two dinitrobenzenesulfonyl moieties and yielded the corresponding bisphenol intermediate, as shown in Figure 7B. Rearrangement of the bisphenol intermediate to the ring-opening of lactone afforded highly fluorescent potassium 2′,4′,5′,7′-tetrafluorofluorescein-10′ (or 11′)-carboxylate regiosisomers (TFFC). The latter compound gave the fluorescence emission at 530 nm (λ_{em}) with the excitation at 484 nm (λ_{ex}). As the probe DNBs-TFFC was not a fluorescent compound, detected emission photon counts were fully associated with the quantity of TFFC produced. Measured total emission intensity counts were then correlated to the relative quantity of O_2^-· generated. As shown in Figure 7Bb, nearly linear progressive increase of fluorescence intensity counts over the full irradiation period was observed that revealed the constant production of O_2^-· from the photoexcited *cis-cup*-**4**-C$_{2M-9}$. As discussed above, continuous irradiation on six DPAF moieties of *cis-cup*-**4**-C$_{2M-9}$ by white LED light (2.0 W) stimulated photoexcitation from the ground to the singlet excited state. Subsequent intramolecular e$^-$-transfer from ^{1}(DPAF-C$_n$)* to <C$_{60}$> moieties resulted in the formation of anionic [60]fullerenyl bisadduct radical (<C$_{60}$>)$^-$ intermediate. In the presence of O$_2$, it was followed by further e$^-$-transfer from (<C$_{60}$>)$^-$ intermediate

to O_2 to produce O_2^- in a sequential multiple-step Type-I photomechanism. These results clearly provided the evidence of photoinduced intramolecular e^--transfer mechanism within the 3D-conformer *cis-cup*-**4**-C_{2M-9}.

Furthermore, one of the main crucial criterion for the use of these types of C_{60}-(light-harvesting antenna)$_n$ conjugates, such as **4**-C_{2M-9}, as the nano-photosensitizers for antibacterial inactivation (aPDI) is their high photostability. Unlike the conventional organic chromophore-based photosensitizers suffering rapid photodegradation, C_{60}-(light-harvesting antenna)$_n$ based nano-drugs were found to be capable of a single dose with multiple aPDI/PDT (photodynamic therapy) treatments [39–42].

3. Experimental Section

3.1. Chemicals and Reagents

Reagents of sodium *t*-butoxide, α-bromoacetyl bromide, aluminum chloride (AlCl$_3$), 1,8-diazabicyclo[5.4.0]undec-7-ene (DBU), *rac*-2,2′-bis(diphenylphosphino)-1,1′-binaphthyl (BINAP), and tris(dibenzylideneacetone)dipalladium(0) [Pd$_2$(dba)$_3$(0)] were purchased from Aldrich Chemicals, Natick, Massachusetts, USA and used without further purification. Fullerene materials with a purity of 99% were purchased from Suzhou Dade Carbon Nanotechnology Co., Ltd. Suzhou, Jiangsu, China. Anhydrous grade solvent of tetrahydrofuran (THF) was used and further dried via refluxing over sodium and benzophenone overnight and distilled under reduced pressure (10^{-1} mmHg). The precursor compounds including 1,3,5-tris(*N*-phenylamino)benzene (TPAB) and 2-bromo-9,9-di(methoxyethyl)fluorene (BrF-C_{2M}) were synthesized according to our previous procedures [34].

3.2. Instruments for Spectroscopic Measurements

^{1}H-NMR spectra were recorded on either Bruker and Spectrospin Avance 500 or Bruker AC-300 spectrometer. UV-vis spectra were recorded on a PerkinElmer *Lambda 750* UV spectrometer. Fluorometric traces were collected using a PTI QuantaMaster^{TM}40 Fluorescence Spectrofluorometer. The light source used in this experiment included a collimated white LED light with an output power of 2.0 W (Prizmatix, Southfield, MI, USA). Infrared spectra were recorded as KBr pellets on a Thermo Nicolet *AVATAR 370* FTIR spectrometer. Cyclic voltammetry (CV) was record on EG&G Princeton Applied Research 263A Potentiostat/Galvanostat using Pt metal as the working electrode, Ag/AgCl as the reference electrode, and Pt wire as the counter electrode at a scan rate of 10 mV/s. The solution for CV measurements was prepared in a concentration of $1.0–5.0 \times 10^{-3}$ M in appropriate solvents containing the electrolyte Bu_4N^+-PF_6^- (0.1 M).

3.3. Synthesis of N^1,N^3,N^5-Tris(9,9-di(methoxyethyl)fluoren-2-yl)-1″,3″,5″-tris(phenylamino)-benzene as Tris(DPAF-C_{2M}) (**2**-C_{2M})

Synthetic procedure for the preparation of tris(DPAF-C_{2M}) was slightly modified from those methods reported recently [34]. In general, a mixture of BrF-C_{2M} (7.33 g, 20.3 mmol, excess), TPAB (1.16 g, 3.3 mmol), and sodium *t*-butoxide (1.94 g, 20.3 mmol) was dissolved in anhydrous toluene (75 mL) and stirred for 1 h to give a homogeneous solution. The catalyst Pd$_2$(dba)$_3$(0) (0.023 g, 0.25 mol%) and *rac*-BINAP (0.046 g, 0.75 mol%) were added to the solution, followed by heating to refluxing temperature under nitrogen for a period of 72 h. After cooling the resulting mixture to room temperature, it was washed with water three times by extraction, the organic layer was separated, and it was dried over sodium sulfate. After solvent evaporation, a small quantity of crude paste was tested on the TLC plate to show the major product at $R_f = 0.6$ using hexane–ethylacetate (1:1, *v/v*) as the eluent. This product spot had a dense yellow-brown color on the top accompanied by a light visible tail. The tail portion was assumed to be the product in the *trans-chair* form. This tail portion was subsequently separated from the main top portion of the *cis-cup* form via column chromatography, followed by the TLC plate purification using silica gel as the stationary phase and hexane-ethylacetate

(1:1, *v/v*) as the eluent to afford the product of *cis-cup*-tris(DPAF-C$_{2M}$) (**2-C$_{2M}$**) as light yellow solids in 82% yield (3.23 g). Verification of the *cis-cup* form was based on the detection of a singlet proton peak at δ6.53 (H$_a$) corresponding to three central core 1,3,5-benzene protons, whereas the trans-chair form gave two proton groups at a integration ratio of 2:1. Spectroscopic data: FT-IR (KBr) v_{max} 3062 (w, aromatic C-H stretching), 3031 (w), 3016 (w), 2969 (w, aliphatic C-H stretching), 2922 (m), 2875 (m), 2814 (w), 1571 (s, C=C), 1491 (s, anti-symmetric deformations of CH$_3$ groups and scissor vibrations of CH$_2$ groups), 1448 (s), 1428 (m), 1381 (w, symmetric deformations of CH$_3$ groups), 1292 (m, asymmetric stretching vibrations of C-N-C), 1248 (m, asymmetric stretching vibrations of C-N-C), 1212 (w), 1176 (w), 1155 (w), 1110 (s, stretching vibrations of C-O-C), 1039 (w), 948 (w), 877 (w), 829 (w), 754 (m), 738 (s, out-of-plan deformation of C-H), 711 (m, out-of-plan deformation of C-H), 692 (s), and 511 (w) cm^{-1}; UV-vis (CHCl$_3$, 1.0×10^{-5} M) λ_{max} (ε) 321 (7.24×10^4 L mol^{-1} cm^{-1}) and 351 nm (7.66×10^4 L mol^{-1} cm^{-1}); ^{1}H NMR (500 MHz, CDCl$_3$) δ 7.58 (s, 3H, br), 7.52 (d, 3H), 7.35–7.24 (m, 9H), 7.15–7.03 (m, 18H), 6.89 (t, 3H), 6.53 (s, 3H, central benzene protons H$_a$), 2.91 (s, 18H), 2.65 (m,12H), and 2.19 (m, 12H).

3.4. Synthesis of N^1,N^3,N^5-Tris(7-α-bromoacetyl-9,9-di(methoxyethyl)fluoren-2-yl)-1″,3″,5″-tris-(phenylamino)benzene as Tris(BrDPAF-C$_{2M}$) (**3-C$_{2M}$**)

The compound *cis-cup*-tris(DPAF-C$_{2M}$) (*cis-cup*-**2-C$_{2M}$**, 0.53 g, 0.44 mmol) was added to a homogeneous suspension of AlCl$_3$ (1.0 g, 7.5 mmol) in 1,2-dichloroethane (40 mL) at 0 °C with vigorous stirring. The reagent α-bromoacetyl bromide (1.0 g, 5.0 mmol) was added slowly over 10 min while maintaining the temperature between 0–10 °C. The mixture was then stirred overnight at room temperature. An excessive amount of AlCl$_3$ remaining in the solution was quenched by slow addition of water (50 mL) while maintaining the temperature below 45 °C. After washing sequentially with dil. HCl (1.0 N, 50 mL) and water (50 mL × 2), the organic layer was separated and dried over sodium sulfate and then concentrated in vacuo to give the crude product as viscous yellow semi-solids. It was purified by column chromatography (silica gel) followed by thin-layer chromatography (TLC) using hexane–EtOAc (1:1, *v/v*) as eluent to afford *cis-cup*-tris(Br-DPAF-C$_{2M}$) (*cis-cup*-**3-C$_{2M}$**) (at R_f = 0.5 on TLC plate) in 48% yield (0.33 g). Spectroscopic data: FT-IR (KBr) v_{max} 3062 (w, aromatic C-H stretching), 3031 (w), 3016 (w), 2969 (w, aliphatic C-H stretching), 2922 (m), 2875 (m), 1673 (s, C=O), 1571 (s, C=C), 1491 (s, anti-symmetric deformations of CH$_3$ groups and scissor vibrations of CH$_2$ groups), 1467 (s), 1448 (s), 1428 (m), 1388 (w), 1348 (w), 1282 (s), 1251 (s), 1195 (m), 1176 (w), 1110 (s, stretching vibrations of C-O-C), 1035 (w), 948 (w), 879 (w), 823 (m), 755 (m), 740 (s, C-H out-of-plan deformation), 715 (m, C-H out-of-plan deformation), 694 (s), 617 (w) and 538 (w) cm^{-1}; UV-vis (CHCl$_3$, 1.0×10^{-5} M) λ_{max} (ε) 310 (7.65×10^4 L mol^{-1} cm^{-1}) and 406 nm (7.91×10^4 L mol^{-1} cm^{-1}); ^{1}H NMR (500 MHz, CDCl$_3$) δ 7.98 (m, 3H), 7.58 (m, 3H), 7.34–7.20 (m, 9H), 7.11–6.98 (m, 18H), 6.96 (m, 3H), 6.56 (m, 3H, aromatic protons of central phenyl ring), 4.49 (m, 6H, α-proton next on C$_{61}$), 2.91 (s, 18H. primary C$_{2M}$ alkyl protons next to O-atom), 2.81–2.50 (centered at δ 2.66, m, 12H, secondary C$_{2M}$ alkyl protons next to O-atom), 2.48–2.07 (centered at δ 2.16, m, 12H, C$_{2M}$ alkyl protons next to the fluorene ring).

3.5. Synthesis of N^1,N^3,N^5-Tris(7-(1,2-dihydro-1,2-methanofullerene[60]-61-carbonyl)-9,9-di(methoxyethyl) fluoren-2-yl)-1″,3″,5″-tris(phenylamino)benzene as Tris[(DPAF-C$_{2M}$)-C$_{60}$(>DPAF-C$_9$)] (**4-C$_{2M–9}$**)

The reagent 1,8-diazabicyclo[5.4.0]undec-7-ene (DBU, 0.21 g, 1.38 mmol) was added slowly to a homogeneous mixture of C$_{60}$>(DPAF-C$_9$) (1.1 g, 0.97 mmol) and *cis-cup*-tris(BrDPAF-C$_{2M}$) (*cis-cup*-**3-C$_{2M}$**, 0.31 g, 0.20 mmol) in anhydrous toluene (700 mL). During the Bingel reaction for the first 2.0 h, the products of mono- and bis-adducts became visible by the TLC technique, showing two brown bands at R_f = ~0.2 and ~0.3, respectively, using a mixture of toluene–EtOAc (7:3, *v/v*) as eluent. After a longer reaction period of 4 h, three brown bands close to each other were observed at R_f = ~0.2, ~0.3, and ~0.4 with the former band progressively becoming faint. At the end of the reaction (8.0 h), only two latter bands remained at R_f = ~0.3 and ~0.4 with the latter as the major chromatographic fraction. At this stage, the reaction mixture was concentrated to a 10% volume and then precipitated

from methanol (100 mL) to afford the crude product mixture, which was isolated by centrifugation. Further purification by column chromatography (silica gel) using toluene to a solvent mixture of toluene–EtOAc (7:3, *v/v*) as the eluent with sequential increments of increasing solvent polarity afforded *cis-cup*-tris[(DPAF-C$_{2M}$)-C$_{60}$(>DPAF-C$_9$)]. It was further purified by TLC with isolation of only the narrow dense color fraction band to give brown solids of *cis-cup*-**4**-C$_{2M-9}$ in 79% yield (0.74 g) (at R_f = ~0.4 on TLC). Spectroscopic data: FT-IR (KBr) ν_{max} 3062 (w, aromatic C-H stretching), 3031 (w), 3016 (w), 2952 (w, aliphatic C-H stretching), 2925 (m), 2852 (w), 1679 (s, C=O), 1591 (s, C=C), 1490 (s, anti-symmetric deformations of CH$_3$ groups and scissor vibrations of CH$_2$ groups), 1465 (s), 1419 (m), 1346 (w), 1315 (m), 1274 (s), 1238 (m), 1211 (s), 1170 (m), 1110 (s, stretching vibrations of C-O-C), 1072 (w), 1029 (w), 950 (w), 879 (w), 815 (m), 746 (s), 694 (s), 574 (w) and 524 (s, <C$_{60}$>) cm^{-1}; UV-vis (CHCl$_3$, 1.0×10^{-5} M) λ_{max} (ε) 296 nm (1.82×10^5 L mol^{-1} cm^{-1}) and 411 nm (1.11×10^5 L mol^{-1} cm^{-1}); ^{1}H NMR (500 MHz, CDCl$_3$) δ 8.65–8.12 (m, 12H, fluorenyl protons next to the keto group), 7.91–7.48 (m, 12H, fluorenyl protons), 7.31−7.06 [m, 57H, 45 aminophenyl protons and 12 fluorenyl protons (2H for each fluorene ring) next to N-atom], 6.57 (m, 3H, aromatic protons of the central phenyl ring), 5.78–5.25 (m, 6H, α-proton next on C$_{61}$), 3.01–2.81 (centered at δ 2.93) (m, 18H, primary C$_{2M}$ alkyl protons next to O-atom), 2.81–2.50 (centered at δ 2.65, m, 12H, secondary C$_{2M}$ alkyl protons next to O-atom), 2.48–2.07 (centered at δ 2.17, m, 12H, C$_{2M}$ alkyl protons next to the fluorine ring), 2.07−1.18 (m, 12H, C$_9$ alkyl protons next to the fluorene ring), 1.18–0.94 (centered at δ 1.14) (m, 6H, tertiary C$_9$ alkyl protons), 0.94–0.30 (centered at δ 0.70) (m, 96H, primary and secondary C$_9$ alkyl protons).

3.6. ROS Measurements Using singlet oxygen ($^1O_2$)-Sensitive Fluorescent Probe

The compound α,α'-(anthracene-9,10-diyl)bis(methylmalonic acid) (ABMA) was used as a fluorescent probe for singlet oxygen ($^1O_2$) trapping. The quantity of $^1O_2$ generated was monitored and counted by the relative intensity decrease of fluorescence emission of ABMA at 428 nm under excitation wavelengths of 380 nm (λ_{ex}). A typical probe solution was prepared by diluting a master solution of ABMA (1.0×10^{-5} M in DMF, 0.4 mL) with an amount 9-fold in volume of CHCl$_3$ (3.2 mL) in a cuvette ($10 \times 10 \times 45$ mm). The solution was added by a pre-defined volume of tris[(DPAF-C$_{2M}$)-C$_{60}$(>DPAF-C$_9$)] in CHCl$_3$ (1.0×10^{-5} M, 0.4 mL), followed by periodic illumination using an ultrahigh power white light LED lamp (Prizmatix, operated at the emission peak maxima centered at 451 and 530 nm with the collimated optical power output of >2.0 W in a diameter of 5.2 cm). Progressive fluorescent spectra were taken on the PTI QuantaMaster^{TM} 40 Fluorescence Spectrofluorometer.

3.7. ROS Measurements Using Superoxide Radical ($O_2^-\cdot$)-Sensitive Fluorescent Probe

A superoxide radical ($O_2^-\cdot$)-reactive fluorescent probe, non-fluorescent potassium bis(2,4-dinitrobenzenesulfonyl)-2',4',5',7'-tetrafluorofluorescein-10' (or 11')-carboxylate regioisomers (DNBs-TFFC), was used for the experiment. A typical probe solution [10^{-6} M in toluene–DMSO (9:1)] was prepared by diluting a stock solution of DNBs-TFFC in DMSO (10^{-5} M, 1.0 mL) by 10 times with toluene (9.0 mL). A dialysis film (CE) with the molecular weight cut-off (MWCO) of 100–500 Da was used to separate the solution of tris[(DPAF-C$_{2M}$)-C$_{60}$(>DPAF-C$_9$)] [10^{-6} M in toluene–DMSO (9:1)] from the probe solution kept in a cuvette with stirring during the fluorescent measurement. Only the solution of **4**-C$_{2M}$ in the membrane sack was subjected to the LED light exposure at the excitation wavelength of 400–700 nm (white light). The quantity of $O_2^-\cdot$ generated was counted in association with its reaction with DNBs-TFFC that resulted in the product of highly fluorescent potassium 2',4',5',7'-tetrafluorofluorescein-10' (or 11')-carboxylate regioisomers (TFFC) with fluorescence emission at 530 nm (λ_{em}) upon excitation at 484 nm (λ_{ex}). The detected intensity increase of fluorescence emission was then correlated to the relative quantity of O_2^- produced.

4. Conclusions

Previous studies on detected photoswitchable dielectric amplification phenomena by the simulated ferroelectric-like capacitor design using the construction and the fabrication of a fullerosome shell layer on core-shell γ-FeO$_x$@AuNPs were based on the photoinduced intramolecular charge-polarization of (C$_{60}$> acceptor)-(DPAF-C$_n$ donor) conjugates [16–18]. The corresponding formation of dielectric ion-radical components (C$_{60}$>)$^-$ and DPAF$^+\cdot$-C$_n$ within a fullerosome array layer was the basis of observed dielectric properties. Accordingly, several such conjugates were developed by the extension from the initial C$_{60}$(>DPAF-C$_9$) to demonstrate the correlation of the structural relationship and the chemical modifications to the enhanced dielectric properties, as stated above. Two interesting modifications both involved 3D-conformeric C$_{60}$(>DPAF-C$_9$) derivatives by fusing three phenyl rings of three diphenylamino groups together to form a shared central benzene moiety as the base of 3D configuration design. Specifically, the successful synthesis of *cis-cup*-tris[(DPAF-C$_{2M}$)-C$_{60}$(>DPAF-C$_9$)] stereoisomer may be beneficial for use as positive (DPAF-C$_n$)$^+$ and negative charge (<C$_{60}$>)$^-$ carriers in enhancing photoinduced dielectric characteristics [43]. It can also be applied as the precursor building block in the synthesis of several C$_{60}$- and C$_{70}$-based ultrafast photoresponsive nonlinear two-photon absorptive nanomaterials. Accordingly, we demonstrated efficient intramolecular energy and electron transfer capabilities of 3D conformer *cis-cup*-**4**-C$_{2M-9}$ using photophysical measurements and its effective production of singlet oxygen (via the energy transfer mechanism) and superoxide radicals (via the electron transfer mechanism). They can be applied as nano-photosensitizers [39–42] and nonlinear photonic agents [30–32,44].

Supplementary Materials: Supplementary Materials can be accessed online.

Author Contributions: All authors contributed significant effort on this work. H.Y. and M.W. carried out the main synthetic works, spectroscopic characterization, data analysis, and physical measurements; L.-S.T., and L.Y.C. participated in the discussion and experimental studies and contributed to a part of manuscript writing; All authors read and approved the final manuscript.

Conflicts of Interest: The authors declare no conflicts of interest.

References

1. El-Khouly, M.E.; Ito, O. Intermolecular and supramolecular photoinduced electron transfer processes of fullerene–porphyrin/phthalocyanine systems. *J. Photochem. Photobiol. C Photochem. Rev.* **2004**, *5*, 79–104.

2. Escudero, D. Revising intramolecular photoinduced electron transfer (PET) from first-principles. *Acc. Chem. Res.* **2016**, *49*, 1816–1824. [CrossRef] [PubMed]

3. Ito, O.; D'Souza, F. Recent advances in photoinduced electron transfer processes of fullerene-based molecular assemblies and nanocomposites. *Molecules* **2012**, *17*, 5816–5835. [PubMed]

4. Wu, W.; Zhao, J.; Sun, J.; Guo, S. Light-harvesting fullerene dyads as organic triplet photosensitizers for triplet–triplet annihilation upconversions. *J. Org. Chem.* **2012**, *77*, 5305–5312. [CrossRef] [PubMed]

5. Ziessel, R.; Allen, B.D.; Rewinska, D.B.; Harriman, A. Selective triplet-state formation during charge recombination in a fullerene/bodipy molecular dyad (bodipy=borondipyrromethene). *Chem. Eur. J.* **2009**, *15*, 7382–7393. [CrossRef] [PubMed]

6. Zhao, J.; Wu, W.; Sun, J.; Guo, S. Triplet photosensitizers: From molecular design to applications. *Chem. Soc. Rev.* **2013**, *42*, 5323–5351. [CrossRef]

7. Chea, Y.; Yuan, X.; Cai, F.; Zhaoa, J.; Zhaoa, X.; Xub, H.; Liu, L. Bodipy−corrole dyad with truxene bridge: Photophysical properties and application in triplet−triplet annihilation upconversion. *Dyes Pigments* **2019**, *171*, 107756. [CrossRef]

8. Kamkaew, A.; Lim, S.H.; Lee, H.B.; Kiew, L.V.; Chung, L.Y.; Burgess, K. BODIPY dyes in photodynamic therapy. *Chem. Soc. Rev.* **2013**, *42*, 77–88. [CrossRef]

9. Natali, M.; Campagna, S.; Scandola, F. Photoinduced electron transfer across molecular bridges: Electron- and hole-transfer superexchange pathways. *Chem. Soc. Rev.* **2014**, *43*, 4005–4018. [CrossRef]

10. Imahori, H.; Sakata, Y. Donor-linked fullerenes: Photoinduced electron transfer and its potential application. *Adv. Mater.* **1997**, *9*, 537–546.

11. D'Souza, F.; Ito, O. Photosensitized electron transfer processes of nanocarbons applicable to solar cells. *Chem. Soc. Rev.* **2012**, *41*, 86–96. [CrossRef] [PubMed]

12. Bottari, G.; Torre, G.; Guldi, D.M.; Torres, T. Covalent and noncovalent phthalocyanine-carbon nanostructure systems: Synthesis, photoinduced electron transfer, and application to molecular photovoltaics. *Chem. Rev.* **2010**, *110*, 6768–6816. [CrossRef] [PubMed]

13. Daly, B.; Ling, J.; Prasanna de Silva, A. Current developments in fluorescent PET (photoinduced electron transfer) sensors and switches. *Chem. Soc. Rev.* **2015**, *44*, 4203–4211. [CrossRef] [PubMed]

14. Yin, R.; Wang, M.; Huang, Y.-Y.; Chiang, L.Y.; Hamblin, M.R. Photodynamic therapy with decacationic [60]fullerene monoadducts: Effect of a light absorbing e⁻-donor antenna and micellar formulation. *Nanomed. Nanotechnol. Biol. Med.* **2014**, *10*, 795–808. [CrossRef] [PubMed]

15. Yin, R.; Wang, M.; Huang, Y.-Y.; Landi, G.; Vecchio, D.; Chiang, L.Y.; Hamblin, M.R. Antimicrobial photodynamic inactivation with decacationic functionalized fullerenes: Oxygen independent photokilling in presence of azide and new mechanistic insights. *Free Radic. Biol. Med.* **2014**, *79*, 14–27. [CrossRef] [PubMed]

16. Segura, J.L.; Martin, N. [60]Fullerene dimer. *Chem. Soc. Rev.* **2000**, *29*, 13–25. [CrossRef]

17. Shirai, Y.; Osgood, A.J.; Zhao, Y.; Kelly, K.F.; Tour, J.M. Directional control in thermally driven single-molecule nanocars. *Nano Lett.* **2005**, *5*, 2330–2334. [CrossRef]

18. Akimov, A.V.; Nemukhin, A.V.; Moskovsky, A.A.; Kolomeisky, A.B.; Tour, J.M. Molecular dynamics of surface-moving thermally driven nanocars. *J. Chem. Theory Comput.* **2008**, *4*, 652–656. [CrossRef]

19. Sasaki, T.; Osgood, A.J.; Kiappes, J.L.; Kelly, K.F.; Tour, J.M. Synthesis of a porphyrin-fullerene pinwheel. *Org. Lett.* **2008**, *10*, 1377–1380. [CrossRef]

20. Zhang, J.; Porfyrakis, K.; Morton, J.J.L.; Sambrook, M.R.; Harmer, J.; Xiao, L.; Ardavan, A.; Briggs, G.A.D.; Briggs, G. Photoisomerization of a fullerene dimer. *J. Phys. Chem.* **2008**, *C 112*, 2802–2904. [CrossRef]

21. Wang, J.L.; Duan, X.F.; Jiang, B.; Gan, L.B.; Pei, J.; He, C.; Li, Y.F. Nanosized rigid π-conjugated molecular heterojunctions with multi[6 0]fullerenes: Facile synthesis and photophysical properties. *J. Org. Chem.* **2006**, *71*, 4400–4410. [CrossRef] [PubMed]

22. López-Andarias, J.; Bauza, A.; Sakai, N.; Frontera, A.; Matile, S. Remote control of anion-π catalysis on fullerene-centered catalytic triads. *Angew. Chem.* **2018**, *130*, 11049–11053. [CrossRef]

23. Sabirov, D.S. Polarizability of C_{60} fullerene dimer and oligomers: The unexpected enhancement and its use for rational design of fullerene-based nanostructures with adjustable properties. *RSC Adv.* **2013**, *3*, 19430. [CrossRef]

24. Pankratyev, E.Y.; Tukhbatullina, A.A.; Sabirov, D.S. Dipole polarizability, structure, and stability of [2+2]-linked fullerene nanostructures $(C_{60})n$ ($n \leq 7$). *Phys. E Low-Dimens. Syst. Nanostruct.* **2017**, *86*, 237–242. [CrossRef]

25. Tukhbatullina, A.; Shepelevich, I.; Sabirov, D.S. Exaltation of polarizability as a common property of fullerene dimers with divers intercage bridges. *Fuller. Nanotub. Carbon Nanostruct.* **2018**, *26*, 661–666. [CrossRef]

26. Swart, M.; van Duijnen, P.T. Rapid determination of polarizability exaltation in fullerene-based nanostructures. *J. Mater. Chem.* **2015**, *C3*, 23–25. [CrossRef]

27. Wang, M.; Su, C.; Yu, T.; Tan, L.-S.; Hu, B.; Urbas, A.; Chiang, L.Y. Novel photoswitchable dielectric properties on nanomaterials of electronic core-shell γ-FeO$_x$@Au@fullerosomes for GHz frequency applications. *Nanoscale* **2016**, *8*, 6589–6599. [CrossRef]

28. Wang, M.; Yu, T.; Tan, L.-S.; Urbas, A.; Chiang, L.Y. Tunability of rf-responses by plasmonic dielectric amplification using branched e⁻-polarizable C_{60}-adducts on magnetic nanoparticles. *J. Phys. Chem. C* **2016**, *120*, 17711–17721. [CrossRef]

29. Wang, M.; Yu, T.; Tan, L.-S.; Urbas, A.; Chiang, L.Y. Enhancement of photoswitchable dielectric property by conducting electron donors on plasmonic core-shell gold-fluorenyl C_{60} nanoparticles. *J. Phys. Chem. C* **2018**, *122*, 12512–12523. [CrossRef]

30. Padmawar, P.A.; Rogers, J.O.; He, G.S.; Chiang, L.Y.; Canteenwala, T.; Tan, L.-S. Large cross-section enhancement and intramolecular energy transfer upon multiphoton absorption of hindered diphenylaminofluorene-C_{60} dyads and triads. *Chem. Mater.* **2006**, *18*, 4065–4074. [CrossRef]

31. Padmawar, P.A.; Canteenwala, T.; Tan, L.-S.; Chiang, L.Y. Synthesis and characterization of photoresponsive diphenylaminofluorene chromophore adducts of [60]fullerene. *J. Mater. Chem.* **2006**, *16*, 1366–1378. [CrossRef]

32. Luo, H.; Fujitsuka, M.; Araki, Y.; Ito, O.; Padmawar, P.; Chiang, L.Y. Inter- and intramolecular photoinduced electron-transfer processes between C$_{60}$ and diphenylaminofluorene in solutions. *J. Phys. Chem. B* **2003**, *107*, 9312–9318. [CrossRef]

33. Hu, R.; Lager, E.; Aguilar-Aguilar, A.; Liu, J.; Lam, J.W.Y.; Sung, H.H.Y.; Williams, I.D.; Zhong, Y.; Wong, K.S.; Pena-Cabrera, E.; et al. Twisted intramolecular charge transfer and aggregation-induced emission of BODIPY derivatives. *J. Phys. Chem. C* **2009**, *113*, 15845–15853. [CrossRef]

34. Kang, N.-G.; Kokubo, K.; Jeon, S.; Wang, M.; Lee, C.-L.; Canteenwala, T.; Tan, L.-S.; Chiang, L. Synthesis and photoluminescent properties of geometrically hindered *cis*-tris(diphenyl-aminofluorene) as precursors to light-emitting devices. *Molecules* **2015**, *20*, 4635–4654. [CrossRef] [PubMed]

35. Lee, Y.-T.; Wang, M.; Kokubo, K.; Kang, N.-G.; Wolf, L.; Tan, L.-S.; Chen, C.-T.; Chiang, L. New 3D-stereoconfigured *cis*-tris(fluorenylphenylamino)-benzene with large steric hindrance to minimize π–π stacking in thin-film devices. *Dyes Pigments* **2018**, *149*, 377–386. [CrossRef]

36. Chiang, L.Y.; Padmawar, P.A.; Canteenwala, T.; Tan, L.-S.; He, G.S.; Kannan, R.; Vaia, R.; Lin, T.-C.; Zheng, Q.; Prasad, P.N. Synthesis of C$_{60}$-diphenylaminofluorene dyad with large 2PA cross-sections and efficient intramolecular two-photon energy transfer. *Chem. Commun.* **2002**, 1854–1855. [CrossRef]

37. Jeon, S.; Wang, M.; Ji, W.; Tan, L.-S.; Cooper, T.; Chiang, L.Y. Broadband two-photon absorption characteristics of highly photostable fluorenyl-dicyanoethylenylated [60]fullerene dyads. *Molecules* **2016**, *21*, 647. [CrossRef]

38. Maeda, H.; Yamamoto, K.; Nomura, Y.; Kohno, I.; Hafsi, L.; Ueda, N.; Yoshida, S.; Fukuda, M.; Fukuyasu, Y.; Yamauchi, Y.; et al. A design of fluorescent probes for superoxide based on a nonredox mechanism. *J. Am. Chem. Soc.* **2005**, *127*, 68–69. [CrossRef]

39. Wang, M.; Huang, L.; Sharma, S.K.; Jeon, S.; Thota, S.; Sperandio, F.F.; Nayka, S.; Chang, J.; Hamblin, M.R.; Chiang, L.Y. Synthesis and photodynamic effect of new highly photostable decacationically armed [60]- and [70]fullerene decaiodide monoadducts to target pathogenic bacteria and cancer cells. *J. Med. Chem.* **2012**, *55*, 4274–4285. [CrossRef]

40. Wang, M.; Maragani, S.; Huang, L.; Jeon, S.; Canteenwala, T.; Hamblin, M.R.; Chiang, L.Y. Synthesis of decacationic [60]fullerene decaiodides giving photoinduced production of superoxide radicals and effective PDT-mediation on antimicrobial photoinactvation. *Eur. J. Med. Chem.* **2013**, *63*, 170–184. [CrossRef]

41. Sperandio, F.F.; Sharma, S.K.; Wang, M.; Jeon, S.; Huang, Y.-Y.; Dai, T.; Nayka, S.; de Sousa, S.C.O.M.; Chiang, L.Y.; Hamblin, M.R. Photoinduced electron-transfer mechanisms for radical-enhanced photodynamic therapy mediated by water-soluble decacationic C$_{70}$ and C$_{84}$O$_2$ fullerene derivatives. *Nanomed. Nanotech. Biol. Med.* **2013**, *9*, 570–579. [CrossRef] [PubMed]

42. Huang, L.; Wang, M.; Huang, Y.-Y.; El-Hussein, A.; Chiang, L.Y.; Hamblin, M.R. Progressive cationic functionalization of chlorin derivatives for antimicrobial photodynamic inactivation and related vancomycin conjugate. *Photochem. Photobiol. Sci.* **2018**, *17*, 638–651. [CrossRef] [PubMed]

43. Yin, H.; Wang, M.; Yu, T.; Tan, L.-S.; Chiang, L.Y. 3D-conformer of tris[60]fullerenylated *cis*-tris(diphenylaminofluorene) as photoswitchable charge-polarizer on GHz-responsive trilayered core-shell dielectric nanoparticles. *Molecules* **2018**, *23*, 1873. [CrossRef] [PubMed]

44. Jeon, S.; Haley, J.; Flikkema, J.; Nalla, V.; Wang, M.; Sfeir, M.; Tan, L.-S.; Cooper, T.; Ji, W.; Hamblin, M.R.; et al. Linear and nonlinear optical properties of light-harvesting hybrid [60]fullerene triads and tetraads with dual NIR two-photon absorption characteristics. *J. Phys. Chem. C* **2013**, *117*, 17186–17195. [CrossRef] [PubMed]

Sample Availability: Sample of tris[(DPAF-C$_{2M}$)-C$_{60}$(>DPAF-C$_9$)] is available from the authors.